Superlattices and Microstructures 139 (2020) 106420

Contents lists available at ScienceDirect

Superlattices and Microstructures

journal homepage: www.elsevier.com/locate/superlattices

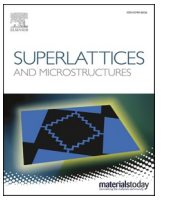

Atomistic simulations of vibration and damping in three-dimensional graphene honeycomb nanomechanical resonators

Bing Li [a,c], Yulan Wei [a], Fanchao Meng [c], Pengfei Ou [c], Yuying Chen [c,d], Lei Che [a], Cheng Chen [b,c,*], Jun Song [c]

[a] School of Engineering, Huzhou University, Huzhou, 313000, China
[b] School of Aeronautics, Northwestern Polytechnical University, Xi'an, 710072, Shaanxi, China
[c] Department of Mining and Materials Engineering, McGill University, Montreal, QC H3A 0C5, Canada
[d] School of Materials Science and Engineering, Harbin Institute of Technology at Weihai, 2 West Wenhua Road, Weihai, 264209, China

ARTICLE INFO

Keywords:
3D graphene honeycombs
Nanomechanical resonators
Vibration characteristics
Damping
Nonlinearity

ABSTRACT

The vibration characteristics and damping of three-dimensional graphene honeycombs (3DGHs) were studied using molecular dynamics simulations and continuum modeling. Both zigzag and armchair 3DGHs were considered. Longitudinal harmonic excitation was applied on the free end of the cantilever honeycomb along the axial direction. Based on the curves of the vibration responses and the amplitude-frequency characteristic of the 3DGH, it was revealed that the amplitude of vibration response and the resonant frequencies of the 3DGHs were influenced by both the excitation frequency and the amplitude of the excitation force. Moreover, the vibration characteristics of the 3DGHs exhibit spring softening nonlinearity, with greater nonlinearity observed as the exciting force increases. The linear and nonlinear damping of the 3DGHs were further evaluated using the loss factor in the sub-resonant regime under various excitation forces, showing that the 3DGH as a resonator can be excited at higher frequencies of GHz with a small loss factor than graphene and CNT. This study demonstrates the relationships of resonant frequencies and damping with the frequency and amplitude of the excitation force in 3DGHs, providing theoretical foundation for designing 3DGH nanomechanical resonators.

1. Introduction

Thanks to their unique and remarkable physical properties, graphene and its derivatives have been extensively investigated and promised unprecedented possibilities for nanotechnology [1–12]. Recently, the advancement in the synthesis of three-dimensional (3D) porous architectures of graphene-based materials, including carbon nanotube (CNT) [13], 3D graphene/nanoparticle aerogel [14], and metal-decorated 3D graphene [15] has furthered their potential applications in energy storage [16–18], biological/medical sensors [19] and semiconductor transistors [20]. Among others, 3D graphene honeycomb (3DGH), being one type of carbon allotrope, has attracted special interest, which has successfully synthetized through depositing vacuum sublimated graphite, and possesses stable lattice structure and exceptional mechanical and physical properties [21–24]. The extensive studies of thermal conductivity and

* Corresponding author. School of Aeronautics, Northwestern Polytechnical University, Xi'an, 710072, Shaanxi, China. Tel.: +86 19871602402.
E-mail address: cheng.chen@nwpu.edu.cn (C. Chen).

https://doi.org/10.1016/j.spmi.2020.106420
Received 9 July 2019; Received in revised form 31 December 2019; Accepted 26 January 2020
Available online 27 January 2020
0749-6036/© 2020 Elsevier Ltd. All rights reserved.

mechanical characteristics of the 3DGH have demonstrated its high capacity for gas storage [21], superior ductility [25] and the best specific strength in 3D carbon nanomaterials [26], and thus enabled the applications as structural composites [27], high thermal conductivity nanodevice [26] and gas adsorption sensors [28].

In addition to the above applications, 3DGH also has great potential for various sensing technology applications, which not only retain the excellent properties of the 2D graphene sheets including high resonant frequencies and remarkable mechanical characteristics [29,30], but provide the geometrical and mechanical flexibility in bulk form, which further enables the diversified manipulation and incorporation in the practical device design, targeting at desirable durability and stability. Therefore, it is expected that 3DGH can serve as a great candidate material for application in nanomechanical resonators and may improve and create new features of nanomechanical sensor. To evaluate the possibility in utilizing 3DGH in nanomechanical resonators, it is of critical importance to study the linear and nonlinear vibration characteristics of 3DGH. However, to date, no systematic studies had been reported on the vibration and damping characteristics of nanomechanical resonators built from 3DGH, particularly on its nonlinear vibration characteristics.

In this work, the characteristics of vibration and damping of 3DGH resonators under the longitudinal harmonic excitation have been investigated by molecular dynamics (MD) simulations combined with continuum modeling. The contents are arranged as the follows. First, two types of 3DGH structures, i.e., zigzag and armchair honeycombs, and their properties are presented. Then, the structure, boundary condition and applied load of the two 3DGH cantilever resonators are specified, followed by a detailed description of simulation methodology. In the last section, the vibration responses, resonant frequencies and nonlinear amplitude-frequency characteristic curves of these two 3DGH resonators are symmetrically explored, and the damping of the 3DGH resonators are evaluated and analyzed.

2. Simulation methodology

The 3DGH structure is composed of arranging and connecting several hexagonal honeycomb units, formed by folding a flat graphene sheet. Two cantilever structures of 3DGH have been constructed and simulated, as shown in Fig. 1. One structure, called zigzag honeycomb, was theoretically proposed by Park and Kuc, which is constructed by arranging *sp* [2]-bonded carbon atoms in the honeycomb unit walls as well as using *sp* [3]-bonded carbon atoms to form junctions between adjacent honeycomb units, as shown in Fig. 1 (a) [31]. This structure is thermodynamically and mechanically stable. The other structure is called armchair honeycomb, where both the wall and junctions of the honeycomb are composed of *sp* [2]-bonded carbon atoms, as depicted in Fig. 1 (b). The armchair honeycomb has been experimentally synthesized and possess remarkable stability [21,31]. Fig. 1 (c) illustrates the Cartesian coordinate system of 3DGH established for our simulations with *X*-axis, *Y*-axis and *Z*-axis being the lattice directions, respectively. The side length of honeycomb unit is equal in order to retain the properties of graphene and is represented using *l*. One end of the 3DGH is clamped as shown in dark red, and the other end is free. After thermally equilibration at target temperature, we apply a series of longitudinal harmonic excitation forces F_z along Z-axial direction to the free end of 3DGH and record the corresponding time-series of axial displacements. F_z, have the form of $F_d\sin(\omega_d t)$, where F_d and ω_d are the amplitude and the angular frequency of the excitation force at the atomic layer of the free end, respectively with $\omega_d = 2\pi f_d$ (f_d is the excitation frequency) [32]. The geometrical dimensions of the 3DGHs are listed in Table 1. Fig. 1 (d) showcases a 3D supercell of 3DGH, where periodic and free boundary conditions were imposed in the lateral (i.e., X and Y) and axial (i.e., Z) directions, respectively.

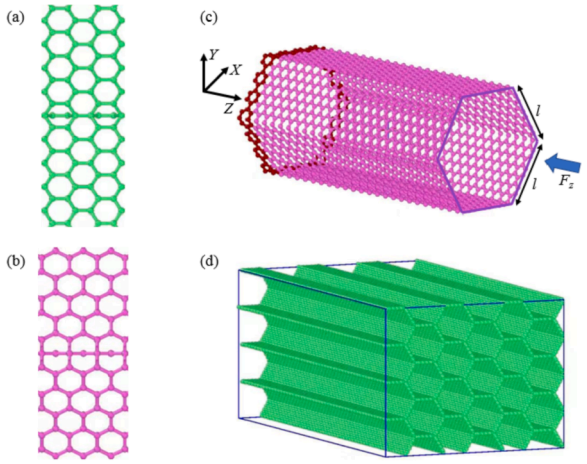

Fig. 1. Structures of 3DGH. The magnified images of atomic construction of a zigzag honeycomb and an armchair honeycomb at junctions are shown in (a) and (b), respectively. As schematic diagram shown in (c), one end of cantilever honeycomb unit is fixed, and the longitudinal harmonic excitation is applied at free end of the honeycomb unit along the honeycomb's axis, where l represents the side length of honeycomb unit, and F_z represents the harmonic excitation force. The periodic and free boundary conditions are used in X/Y and Z, respectively, as shown in (c). An integral simulation model of 3DGH resonator is cuboid and a typical three-dimension structure of 3DGH is shown in (d).

Classical MD simulations are performed using the LAMMPS package [33], employing the adaptive intermolecular reactive empirical bond order (AIREBO) potential [34]. The AIREBO potential has been demonstrated to correctly predict mechanical and physical properties of various C-based structures [31,35,36]. In all MD simulations, the honeycombs constructed are first minimized at 0 K through the conjugate gradient algorithm [37–39], and then relaxed within the isothermal-isobaric (NPT) ensemble at 300 K over a duration of 1 ns to ensure zero stress conditions along all directions [40]. Subsequently, the canonical NVT ensemble has been applied to simulate the vibration properties of honeycomb models subjected various axial harmonic excitation forces at the free end of the structures. The timestep of 1 fs (fs) has been set for all simulations.

3. Results and discussion

The vibration responses of 3DGH is characterized by the axial displacements of the atomic layer at the free end of 3DGH. Fig. 2 shows the vibration responses of the 3DGHs with different excitation forces at an excitation frequency of 215 GHz. It is seen that when $F_z = 0$, The fluctuation response is all from thermomechanical noise. While with the increase of F_z, the vibration response is composed of both thermomechanical noise and harmonic response, and the harmonic response is gradually enhanced with the increase of the excitation force. Moreover, the proportion of thermal noise in vibration response decreases as the excitation force increases, and the nonlinear vibration response arises when the exciting force is further increased. For example, the peak amplitudes of vibration response of these two 3DGHs are more than 50 times bigger than the thermomechanical noise when the amplitude of the excitation force is 16.8 GPa. In addition, the amplitudes of vibration responses show the nonlinear characteristics of the zigzag honeycomb at the excitation force of 8.4 GPa and of the armchair honeycomb at the excitation force of 16.8 GPa.

In addition, the thermomechanical noise amplitudes of these two 3DGHs are very close when the excitation force is equal to zero. However, there is a difference in the amplitude of vibration response when the longitudinal harmonic excitation is applied. This difference becomes larger as the amplitude of the excitation force increases. The amplitude of vibration response of the zigzag honeycomb is larger than that of the armchair honeycomb under the same amplitude of the excitation force and excitation frequency (215 GHz), and. Furthermore, there is a relatively big difference in the amplitude of vibration response of these two 3DGHs when the excitation force is 8.4 GPa, because the zigzag honeycomb produces resonance while the armchair honeycomb does not. This finding suggests that the resonant frequency of these two 3DGHs are different at the excitation force of 8.4 GPa and the excitation frequency of 215 GHz.

The cross-sectional shapes of the two types of 3DGHs under the maximum excitation force are shown in Fig. 3. Viewing from the *Z*-axis direction, the walls of the honeycomb show a buckle state with the increase of the excitation force. Furthermore, the deformation of the zigzag honeycomb is larger than that of the armchair honeycomb at the same excitation force and excitation frequency, because the Young's modulus of the former is smaller than that of the latter. Above results are consistent with the deformation process of the honeycomb under the axial static load [31].

The amplitude-frequency characteristic curve can be obtained by performing fast Fourier transform (FFT) of the recorded time-series of axial vibration responses in frequency domain [41]. As shown in Fig. 4, the amplitude-frequency characteristic curves of the 3DGHs are expressed. This curve expresses the relationship between the excitation frequency and the vibration amplitude. There are some prominent peaks in the curve of both honeycombs, where the frequency corresponds to the resonant frequency. The amplitude of the vibration reaches the maximum value when the resonance occurs. Meanwhile, in addition to the excitation frequency, the amplitude-frequency characteristic curve is also affected by the amplitude of the excitation force. As the excitation force increases, the vibration amplitude of the 3DGHs increases and the resonant frequency decreases.

In addition, the amplitude-frequency characteristic curve of both 3DGHs exhibits nonlinear characteristic. In this work, the nonlinear amplitude-frequency characteristic curves of these two 3DGHs present the spring softening nonlinearity, as shown in Fig. 4. The larger the exciting force, the greater the nonlinearity. This nonlinearity is extremely evident in the frequency range of the resonance region. However, the effect of the nonlinearity on vibration can be ignored in the non-resonant region, because the vibration amplitudes in the non-resonant region are far less than those in the resonance region. The resonant frequencies of the 3DGHs under different longitudinal harmonic excitation forces are shown in Table 2.

However, the amplitude-frequency characteristic curves of the two types of honeycombs also exhibits distinctions. It is found that under the same excitation force, the resonant frequency of the zigzag honeycomb is lower than that of the armchair honeycomb, but the peak amplitude of the former's vibration at the resonant frequency is larger than that of the latter. Moreover, as the excitation frequency increases, the nonlinearity of the former occurs earlier than the latter. Therefore, the nonlinearity of the zigzag honeycomb is stronger than that of the armchair honeycomb.

To quantify the damping of the 3DGH, we further calculated the loss factor by analyzing and calculating the vibration response and amplitude-frequency characteristic curves of the honeycomb in the sub-resonant regime based on the method of Kunal and Aluru [42]. The excitation force produces work done. The rate of the energy dissipation can be evaluated according to the work done at each unit time. The temperature and the internal energy of a microcanonical ensemble is promoted because of the role of this work done.

Table 1
Geometrical parameters and mechanical properties of 3DGHs.

Honeycomb Structure	Length (L)	Cross-Section	Side Length of Honeycomb Unit (l)	Axial Stiffness (k_z)	Young's Modulus (E)
Zigzag	20.9 nm	11.1 nm × 8.6 nm	1.25 nm	1082 N/m	238Gpa
Armchair	21.8 nm	12.6 nm × 9.7 nm	1.4 nm	1433 N/m	258Gpa

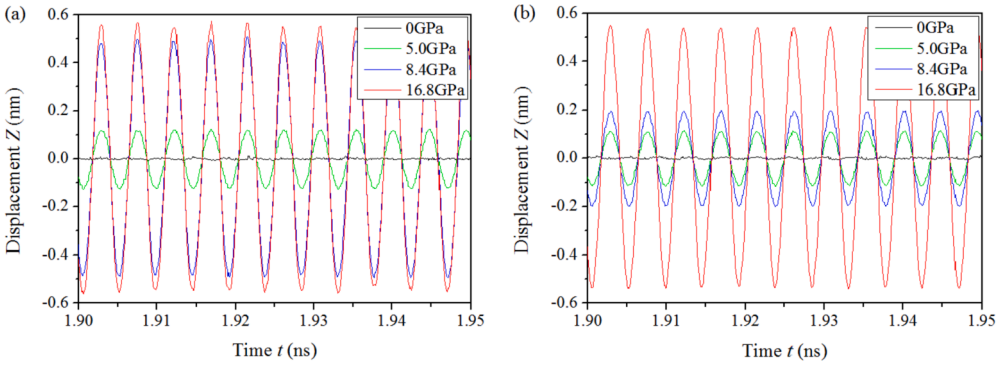

Fig. 2. Vibration responses at the free end of (a) a zigzag honeycomb and (b) an armchair honeycomb. The vibration response curves are presented in green, blue and red when the longitudinal harmonic excitation force with amplitudes of 5.0 GPa, 8.4 GPa and 16.8 GPa are used, respectively. The excitation frequency is 215 GHz for all the simulations.

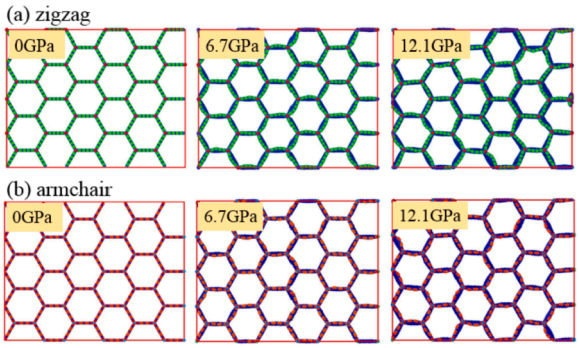

Fig. 3. Atomic configurations of the zigzag (a) and armchair (b) honeycombs viewed along the *Z*-axis direction under longitudinal harmonic excitation force with amplitudes of 0 GPa, 6.7 GPa and 12.1 GPa, respectively.

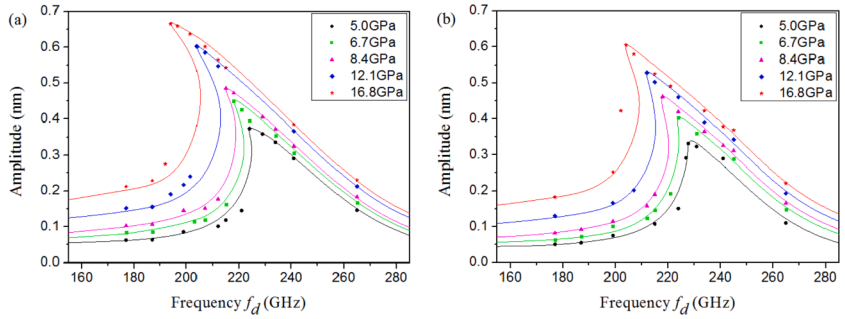

Fig. 4. Nonlinear amplitude-frequency characteristic curves of (a) a zigzag honeycomb and (b) an armchair honeycomb. The nonlinear amplitude-frequency curves are presented in black, green, purple, blue and red when the longitudinal harmonic excitation force with amplitudes of 5.0 GPa, 6.7 GPa, 8.4 GPa, 12.1 GPa and 16.8 GPa, respectively. The range of the excitation frequencies is from 155 GHz to 285 GHz for all the simulations.

Table 2
Resonant frequencies of the 3DGHs.

Honeycomb structure	5.0 GPa	6.7 GPa	8.4 GPa	12.1 GPa	16.8 GPa
Zigzag (GHz)	224	218	215	204	194
Armchair (GHz)	228	224	218	212	204

Therefore, the dissipated energy in unit time W_d can be calculated in Equation (1) [41–43].

$$W_d = \frac{1}{f_d T_n} \int_0^{T_n} F_d v_z \sin(\omega_d t) dt \tag{1}$$

where T_n is the overall time of work done, and v_z is the atomic velocity of Z-axis. The stored energy W_s can be calculated in Equation (2) [41–43].

$$W_s = \frac{1}{2} k_z A_z^2 \tag{2}$$

where k_z is the stiffness of the Z-axis, and A_z is the peak amplitude of the Z-axial vibration. A_z can be obtained in Equation (3) [41–43].

$$A_z = 2 \times \frac{\max\{\mathrm{abs}[\mathrm{FFT}(R_z)]\}}{n_d} \tag{3}$$

where, R_z is the data of the Z-axial vibration response at the center of free end's atomic layer, and the total amount of the data points is defined as n_d when these data are performed by FFT.

Therefore, the loss factor η is computed in Equation (4) [41–43].

$$\eta = \frac{W_d}{2\pi \times W_s} \tag{4}$$

The loss factors at the temperature of 300 K for the longitudinal harmonic vibration of the zigzag and armchair honeycombs are shown in Table 3. In sub-resonant regime, i.e., when the excitation forces vary from 1.7 GPa to 5.0 GPa, the differences between loss factors of zigzag and loss factors of armchair are relatively small. Nonlinear vibration affects the damping of the 3DGHs. The nonlinear damping of the zigzag and armchair honeycombs, i.e., with the excitation forces ranging from 5.9 GPa to 8.4 GPa, the differences between loss factors of zigzag and armchair become larger as the excitation force increases beyond the linear regime. The greater the excitation force, the larger the difference. The difference is 19% for the zigzag and armchair honeycombs under the excitation force of 8.4 GPa. Furthermore, under the same excitation frequency and amplitude of excitation force, the damping of the zigzag honeycomb is larger than that of armchair honeycomb.

A comparison of the loss factors of the 3DGHs with the previous results for the graphene and CNT presented in Refs. [44–46] has shown that their loss factors are comparable ranging from 10^{-2} to 10^{-4}. The temperatures are the same (300 K) in these studies. High resonant frequency combined with low loss factor is a significant performance indicator for application of nanomechanical resonator. At room temperature, the 3DGHs as resonator can be excited at higher frequencies of GHz with a small loss factor than graphene and CNT. The loss factor of the 3DGHs are strongly changed by the excitation force, which is in good agreement with the conclusion of the loss factor for graphene and CNT in previous studies [44–46].

Moreover, the 3DGHs resonators have strong covalently bonded configuration and thus possess superior specific strength and ultra-high stretch ability along all three directions, thus enhanced stability and durability could be achieved with a wide range of excitation forces and ultra-high excitation frequencies (GHz) compared with traditional graphene and CNT resonators [26,47,48]. In addition, flexible structural tailoring could be further performed to obtain 3DGHs resonators with various geometries and easy to be directly used in practical 3D nanodevices, which is better than the doubly clamped graphene resonators of low-dimensional membrane geometric structure.

4. Conclusions

In summary, we explored the vibration characteristics and damping of two types of 3DGHs, i.e., zigzag and armchair honeycombs, under longitudinal harmonic excitation using continuum modeling and atomistic simulations.

4.1. Vibration characteristics

The axial stiffness and the Young's modulus of these two 3DGHs are received by static tensile simulations. The vibration response curves and properties of fluctuation, linear vibration and nonlinear vibration of these two honeycombs are presented under the longitudinal harmonic excitation at the atomic layers of the 3DGHs' free end. The amplitude of vibration response is gradually enhanced with the excitation force increasing, and the nonlinear vibration appears when the exciting force is further increased. The amplitude of vibration response of the zigzag honeycomb is larger than the one of armchair honeycomb on the condition of the same exciting force. The projection views of 3DGH's sectional deformation have been illustrated under various excitation forces. The amplitude-frequency characteristic curves of the 3DGHs are shown, which are influenced by the excitation frequency as well as the amplitude of the excitation force. As the excitation force increases, the resonant frequencies of the 3DGHs decreases. The amplitude-frequency characteristic curve of the 3DGHs exhibits nonlinear characteristics when the exciting force is further increased. The larger the exciting force, the greater the nonlinearity. Moreover, the nonlinearity of the 3DGHs presents the spring softening nonlinearity. The nonlinear influence on vibration is obvious in the resonance region. However, the effect of the nonlinearity on vibration can be ignored in the non-resonant region due to the small vibration amplitude. Besides, under the same excitation force, the resonant frequency of the zigzag honeycomb is lower than that of the armchair honeycomb, but the peak amplitude of vibration of the former at the

Table 3
Loss factors at 300 k for zigzag and armchair honeycombs.

Honeycomb structure	Excitation frequency f_d (GHz)	Force F_d (GPa)	Loss factors η
Zigzag	10	1.7	1.14×10^{-2}
		3.4	2.27×10^{-2}
		5.0	2.90×10^{-2}
		5.9	3.44×10^{-2}
		8.4	3.84×10^{-3}
Armchair	10	1.7	1.09×10^{-2}
		3.4	2.10×10^{-2}
		5.0	2.61×10^{-2}
		5.9	2.88×10^{-2}
		8.4	3.11×10^{-3}

resonant frequency is larger than that of the latter. Therefore, the nonlinearity of the zigzag honeycomb is stronger than that of the armchair honeycomb.

4.2. Loss factors

The loss factors have been evaluated through calculating dissipated and stored energies during the variation of 3DGHs' based on the energy-dissipation mechanism, which determine the damping characteristics of 3DGH in the sub-resonant regime. Under various amplitudes of excitation force, the loss factors of the zigzag and armchair honeycombs are received at the temperature of 300 K in 10 GHz for the longitudinal harmonic vibration. The errors between the loss factors of zigzag and loss factors of armchair are compared in linear and nonlinear vibration. Under the same excitation frequency and amplitude of excitation force, the loss factor of the zigzag honeycomb is larger than that of armchair honeycomb. Furthermore, the loss factors of the 3DGHs can be adjusted by varying the excitation force, which is valuable in both practical application and theoretical study.

The authors declare that they have no conflict of interest.

CRediT authorship contribution statement

Bing Li: Conceptualization, Writing - original draft. **Yulan Wei:** Writing - original draft. **Fanchao Meng:** Investigation, Methodology. **Pengfei Ou:** Formal analysis. **Yuying Chen:** Formal analysis. **Lei Che:** Writing - review & editing. **Cheng Chen:** Supervision, Writing - original draft. **Jun Song:** Conceptualization, Writing - review & editing.

Acknowledgments

We greatly acknowledge the financial support from China Scholarship Council (No. 201708330107 and 201306290017), National Natural Science Foundation of China (51704243 and 5164205), McGill Engineering Doctoral Award, and Natural Sciences and Engineering Research Council of Canada (NSERC) Discovery grant (grant # RGPIN-2017-05187). We also thank Supercomputer Consortium Laval UQAM, McGill, and Eastern Quebec for providing computing power.

References

[1] M.J. Allen, V.C. Tung, R.B. Kaner, Chem. Rev. 110 (2010) 132.
[2] B. Li, P.F. Ou, Y.L. Wei, X. Zhang, J. Song, Materials 11 (2018).
[3] D. Akinwande, C.J. Brennan, J.S. Bunch, P. Egberts, J.R. Felts, H.J. Gao, R. Huang, J.S. Kim, T. Li, Y. Li, K.M. Liechti, N.S. Lu, H.S. Park, E.J. Reed, P. Wang, B. I. Yakobson, T. Zhang, Y.W. Zhang, Y. Zhou, Y. Zhu, Extrem. Mech. Lett. 13 (2017) 42.
[4] W.W. Liu, S.P. Chai, A.R. Mohamed, U. Hashim, J. Ind. Eng. Chem. 20 (2014) 1171.
[5] Q.L. Fang, Y. Shen, B.L. Chen, Chem. Eng. J. 264 (2015) 753.
[6] S. Sadeghzadeh, M.M. Khatibi, Superlattice. Microst. 117 (2018) 271.
[7] H. Abdelsalam, V.A. Saroka, W.O. Younis, Superlattice. Microst. 129 (2019) 54.
[8] B.L. Li, T. Liu, D.W. Hewak, Q.J. Wang, Superlattice. Microst. 113 (2018) 401.
[9] S.W. Wang, B.C. Yang, H.Y. Chen, E. Ruckenstein, J. Mater. Chem. 6 (2018) 6815.
[10] X. He, L. Gao, N. Tang, J.X. Duan, F.J. Xu, X.Q. Wang, X.L. Yang, W.K. Ge, B. Shen, Appl. Phys. Lett. 105 (2014).
[11] X. He, N. Tang, X.X. Sun, L. Gan, F. Ke, T. Wang, F.J. Xu, X.Q. Wang, X.L. Yang, W.K. Ge, B. Shen, Appl. Phys. Lett. 106 (2015).
[12] D.H. Wu, B.C. Yang, H.Y. Chen, E. Ruckenstein, Energy Storag. Mater. 16 (2019) 574.
[13] M.Q. Zhao, X.F. Liu, Q. Zhang, G.L. Tian, J.Q. Huang, W.C. Zhu, F. Wei, ACS Nano 6 (2012) 10759.
[14] W.F. Chen, S.R. Li, C.H. Chen, L.F. Yan, Adv. Mater. 23 (2011) 5679.
[15] H.J. Huang, S.B. Yang, R. Vajtai, X. Wang, P.M. Ajayan, Adv. Mater. 26 (2014) 5160.
[16] E. Yoo, H.S. Zhou, ACS Nano 5 (2011) 3020.
[17] J.X. Zhu, X.Y. Guo, H. Wang, W.X. Song, J. Mater. Sci. 53 (2018) 12413.
[18] S.W. Wang, Z.R. Chen, B.C. Yang, H.Y. Chen, E. Ruckenstein, J. Colloid Interface Sci. 555 (2019) 431.
[19] Y.X. Huang, X.C. Dong, Y.X. Liu, L.J. Li, P. Chen, J. Mater. Chem. 21 (2011) 12358.
[20] H.L. Xu, Z.Y. Zhang, Z.X. Wang, S. Wang, X.L. Hang, L.M. Peng, ACS Nano 5 (2011) 2340.
[21] N.V. Krainyukova, E.N. Zubarev, Phys. Rev. Lett. 116 (2016).
[22] J. Zhang, Carbon 131 (2018) 127.
[23] J. Zhang, Meccanica 53 (2018) 2999.

[24] S.W. Wang, D.H. Wu, B.C. Yang, E. Ruckenstein, H.Y. Chen, Nanoscale 10 (2018) 2748.
[25] X.K. Gu, Z.Q. Pang, Y.J. Wei, R.G. Yang, Carbon 119 (2017) 278.
[26] Z.Q. Pang, X.K. Gu, Y.J. Wei, R.G. Yang, M.S. Dresselhaue, Nano Lett. 17 (2017) 179.
[27] C.Y. Zhong, Y.P. Chen, Y.E. Xie, S.Y.A. Yang, M.L. Cohen, S.B. Zhang, Nanoscale 8 (2016) 7232.
[28] Y. Gao, Y.P. Chen, C.Y. Zhong, Z.W. Zhang, Y.E. Xie, S.B. Zhang, Nanoscale 8 (2016) 12863.
[29] R.A. Barton, B. Ilic, A.M. van der Zande, W.S. Whitney, P.L. McEuen, J.M. Parpia, H.G. Craighead, Nano Lett. 11 (2011) 1232.
[30] C.Y. Chen, S. Rosenblatt, K.I. Bolotin, W. Kalb, P. Kim, I. Kymissis, H.L. Stormer, T.F. Heinz, J. Hone, Nat. Nanotechnol. 4 (2009) 861.
[31] F.C. Meng, C. Chen, D.Y. Hu, J. Song, J. Mech. Phys. Solid. 109 (2017) 241.
[32] A. Pedrielli, S. Taioli, G. Garberoglio, N.M. Pugno, Carbon 116 (2017) 20.
[33] S. Plimpton, J. Comput. Phys. 117 (1995) 1.
[34] S.J. Stuart, A.B. Tutein, J.A. Harrison, J. Chem. Phys. 112 (2000) 6472.
[35] T. Zhang, X.Y. Li, H.J. Gao, Extrem. Mech. Lett. 1 (2014) 3.
[36] T. Zhang, X.Y. Li, S. Kadkhodaei, H.J. Gao, Nano Lett. 12 (2012) 4605.
[37] C. Chen, F.C. Meng, J. Song, J. Appl. Phys. 117 (2015).
[38] C. Chen, P.F. Song, F.C. Meng, P.F. Ou, X.Y. Liu, J. Song, Appl. Phys. Lett. 113 (2018).
[39] NJ, WSJ, Numerical Optimization, second ed., 2006, p. 101.
[40] C. Chen, F.C. Meng, P.F. Ou, G.Q. Lan, B. Li, H.C. Chen, Q.W. Qiu, J. Song, J. Phys. Condens. Matter 31 (2019).
[41] Z. Nourmohammadi, S. Mukherjee, S. Joshi, J. Song, S. Vengallatore, J. Microelectromech. Syst. 24 (2015) 1462.
[42] K. Kunal, N.R. Aluru, Phys. Rev. B 84 (2011).
[43] S. Mukherjee, J. Song, S. Vengallatore, Model. Simulat. Mater. Sci. Eng. 24 (2016).
[44] S.K. Georgantzinos, G.I. Giannopoulos, D.E. Katsareas, P.A. Kakavas, N.K. Anifantis, Comput. Mater. Sci. 50 (2011) 2057.
[45] N. Kacem, S. Hentz, D. Pinto, B. Reig, V. Nguyen, Nanotechnology 20 (2009).
[46] V. Sazonova, Y. Yaish, H. Ustunel, D. Roundy, T.A. Arias, P.L. McEuen, Nature 431 (2004) 284.
[47] Y. Liu, J.J. Liu, S.F. Yue, J.Q. Zhao, B. Ouyang, Y.H. Jing, Physica Status Solidi B-Basic Solid State Phys. 255 (2018).
[48] Z. Zhang, A. Kutana, Y. Yang, N.V. Krainyukova, E.S. Penev, B.I. Yakobson, Carbon 113 (2017) 26.